Comparison of ^{18}F-FDG and PiB PET in Cognitive Impairment

Val J. Lowe[1], Bradley J. Kemp[1], Clifford R. Jack, Jr.[1], Matthew Senjem[2], Stephen Weigand[3], Maria Shiung[1], Glenn Smith[4], David Knopman[5], Bradley Boeve[5], Brian Mullan[1], and Ronald C. Petersen[5]

[1]Department of Radiology, Mayo Clinic, Rochester, Minnesota; [2]Department of Information Technology, Mayo Clinic, Rochester, Minnesota; [3]Department of Health Sciences Research, Mayo Clinic, Rochester, Minnesota; [4]Department of Psychology, Mayo Clinic, Rochester, Minnesota; and [5]Department of Neurology, Mayo Clinic, Rochester, Minnesota

The purpose of this study was to compare the diagnostic accuracy of glucose metabolism and amyloid deposition as demonstrated by ^{18}F-FDG and Pittsburg Compound B (PiB) PET to evaluate subjects with cognitive impairment. **Methods:** Subjects were selected from existing participants in the Mayo Alzheimer's Disease Research Center or Alzheimer's Disease Patient Registry programs. A total of 20 healthy controls and 17 amnestic mild cognitive impairment (aMCI), 6 nonamnestic mild cognitive impairment (naMCI), and 13 Alzheimer disease (AD) subjects were imaged with both PiB and ^{18}F-FDG PET between March 2006 and August 2007. Global measures for PiB and ^{18}F-FDG PET uptake, normalized to cerebellum for PiB and pons for ^{18}F-FDG, were compared. Partial-volume correction, standardized uptake value (SUV), and cortical ratio methods of image analysis were also evaluated in an attempt to optimize the analysis for each test. **Results:** Significant discrimination ($P < 0.05$) between controls and AD, naMCI and aMCI, naMCI and AD, and aMCI and AD by PiB PET measurements was observed. The paired groupwise comparisons of the global measures demonstrated that PiB PET versus ^{18}F-FDG PET showed similar significant group separation, with only PiB showing significant separation of naMCI and aMCI subjects. **Conclusion:** PiB PET and ^{18}F-FDG PET have similar diagnostic accuracy in early cognitive impairment. However, significantly better group discrimination in naMCI and aMCI subjects by PiB, compared with ^{18}F-FDG, was seen and may suggest early amyloid deposition before cerebral metabolic disruption in this group.

Key Words: PET; dementia; ^{18}F-FDG; PiB

J Nucl Med 2009; 50:878–886
DOI: 10.2967/jnumed.108.058529

Imaging that can detect functional or pathophysiologic change in the brain holds great promise for diagnostic and therapy assessment uses in patients with Alzheimer disease (AD). ^{18}F-FDG PET can identify patients with a high potential to convert from mild cognitive impairment (MCI), a prodromal stage of neurodegenerative disease, to AD and predict development of AD in elderly patients and other cognitively healthy high-risk groups (*1,2*). Clinical studies with ^{18}F-FDG PET suggest that the likelihood of a clinical response to therapy can be predicted by ^{18}F-FDG uptake (*3*), and ^{18}F-FDG PET has been used successfully in phase I neurogenesis trials (*4*).

Amyloid plaques have been imaged in the human brain using Pittsburg Compound B (PiB) PET (*5*). The specific pattern of uptake of PiB in human AD subjects has been demonstrated to represent the typical distribution of amyloid-affected regions of the brain, as observed pathologically (*6–9*). Therefore, PiB PET may offer improved accuracy in the characterization of subjects with memory complaints and may aid in antiamyloid therapy trials.

It has been shown that cortical PiB binding levels in healthy elderly volunteers can be as high as those in AD subjects (*10*). The significance of this finding is not yet certain, as longitudinal data are still being collected, but 2 possible explanations are nonpathologic amyloid accumulation or preclinical disease amyloid deposition. Recent data have also shown that MCI subjects with PiB accumulation are more likely to convert to AD than those without (*11*). ^{18}F-FDG and PiB appear, then, to have similar predictive value in this regard, thus warranting a comparison of PiB and ^{18}F-FDG imaging in early neurodegenerative disease.

MCI subjects provide an interesting group in which to investigate the early deposition of brain amyloid. Nevertheless, not all MCI subjects convert to AD. There are notably several subtypes of MCI, some of which may be less likely to progress to probable AD. On both ^{18}F-FDG and PiB, MCI subjects show variable imaging abnormalities, which may reflect the heterogeneous nature of the cohort. Therefore, we included in this evaluation a subset of nonamnestic MCI (naMCI) subjects who may be less at risk for development of AD than amnestic MCI (aMCI) subjects (*12,13*) and may provide better test-group stratification for evaluating imaging characterization accuracy in the MCI group.

A recent report has described a slightly poorer performance for ^{18}F-FDG, compared with PiB, in characterizing early dementia (*14*). To further investigate this paradigm, in

Received Oct. 16, 2008; revision accepted Feb. 12, 2009.
For correspondence or reprints contact: Val J. Lowe, Mayo Clinic, 200 First St. SW, Rochester, MN 55905.
E-mail: vlowe@mayo.edu

this project we evaluated the comparative diagnostic performance of PiB and ^{18}F-FDG scans in several early cognitive impairment subtypes. In the data analysis, we also attempted to determine the optimal analysis method for each modality. Many PiB data analyses published to date have reported their results in terms of cortical-to-reference ratios, also known as standardized uptake value ratios (SUVRs) (*15*). In the wider field of PET body imaging, the standardized uptake value (SUV) is a ratio of the regional activity to a subject-specific scale factor, determined by the injected dose and the patient body weight. In this project, we compared this traditional SUV approach with the results of the alternative SUVR method in ^{18}F-FDG and PiB imaging. The use of dose- and weight-normalized SUV measurements could provide an alternative to cortical ratios in situations in which a standard reference tissue may be suggestive, such as in subjects who may accumulate amyloid in the cerebellum (as can occasionally occur in some familial AD subtypes) (Fig. 1) (*16–18*). Rarely, amyloid deposition in the cerebellum can also be seen in sporadic AD (*19*). Both partial-volume correction (PVC) and nonpartial-volume correction of the PiB and ^{18}F-FDG data were also evaluated. ^{18}F-FDG and PiB PET were then compared in terms of their ability to characterize different groups of subjects with and without cognitive impairment.

MATERIALS AND METHODS

Subject Recruitment

This study was approved by our Institutional Review Board. All subjects, including the healthy controls, were recruited through the Alzheimer's Disease Research Center and the Alzheimer's Disease Patient Registry, Mayo Clinic. Healthy elderly subjects with no cognitive impairment (n = 20), subjects with amnestic MCI (aMCI) (n = 17), subjects with nonamnestic MCI (naMCI) (n = 6), and subjects with mild probable AD (n = 13) were recruited. Subjects with mild probable AD were diagnosed according to DSM-III-R (*20*) criteria for dementia and National Institute of Neurological and Communicative Disorders and Stroke and the Alzheimer's Disease and Related Disorders Association criteria for AD (*21*), and subjects with aMCI and naMCI were classified according to consensus criteria (*22*). Subjects with structural abnormalities and addictions, psychiatric diseases, or treatments that would affect cognitive function were not included.

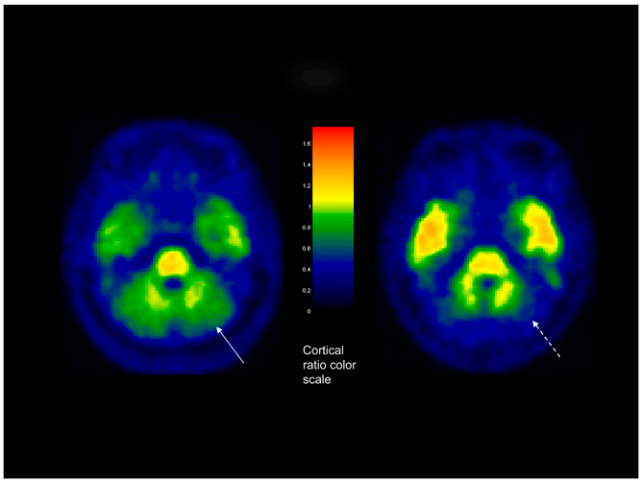

FIGURE 1. Axial PiB brain image (left) in 72-y-old male subject in study group, with clinical diagnosis of AD, showing PiB accumulation in GM region of cerebellum (arrow). Image on right shows different AD subject with no PiB accumulation in GM region of cerebellum (dashed arrow).

Neuropsychological Testing

Cognitive testing was completed within 4 mo of the PET scans. All of the subjects received identical clinical and neurocognitive evaluations, and all were staged according to the Clinical Dementia Rating (CDR) scale (*23*). The controls and MCI subjects in the current study were classified as CDR 0 and CDR 0.5, respectively, and the AD subjects were classified as either CDR 0.5 or CDR 1.0. Memory was evaluated by free recall percentage retention scores computed after a 30-min delay for the Wechsler Memory Scale-Revised Logical Memory, Visual Reproduction subtests and the Rey Auditory Verbal Learning Test. Language tests measured confrontation naming and category fluency. The attention or executive measures included the Trail Making Test, parts A and B, and the Wechsler Adult Intelligence Scale-Revised (WAIS-R) Digit Symbol subtest. Visuospatial processing was examined by the WAIS-R Picture Completion and Block Design subtests. All tests were administered by experienced psychometrists and supervised by board-certified clinical neuropsychologists. All raw scores were converted to Mayo Older American Normative Studies (MOANS) age-adjusted scaled scores that are normally distributed and that have a mean of 10 and a SD of 3 in cognitively healthy subjects on whom each test was based (*24*). In each cognitive domain, a mean MOANS age-corrected scaled score was computed for every participant.

Consensus Diagnosis of MCI Subjects

A final consensus diagnosis of MCI subjects was made by a panel (nurse, psychometrist, neuropsychologist, and neurologist) that considered historical, clinical, and neuropsychologic data comprehensively. The subjects' mean MOANS scores within a certain domain did not strictly define their MCI category, although cognitive tests were used to inform the clinical consensus diagnosis. Subjects were classified as aMCI if the impairment included only the memory domain on the consensus diagnosis or if the impairment was in the memory domain plus 1 or more other domains such as language, attention or executive function, and visuospatial processing (multidomain). A classification of naMCI was assigned when impairment included 1 or more nonmemory domains with relative preservation of memory.

PET

PET images were acquired using 1 of 2 PET/CT scanners (DRX; GE Healthcare) operating in 3-dimensional mode (septa removed). The subjects were injected with PiB (average, 596 MBq; range, 292–729 MBq) and ^{18}F-FDG (average, 540 MBq; range, 366–399 MBq) on the same day with 1 h between the PiB and the PET scan acquisitions. Subjects were prepared for ^{18}F-FDG in a dimly lit room, with minimal auditory stimulation. A CT image was obtained for attenuation correction. After a 40-min (PiB) or 30-min (^{18}F-FDG) uptake period, the subjects were

imaged. A 20-min PiB or an 8-min ^{18}F-FDG scan was obtained. The PiB PET acquisition consisted of four 5-min dynamic frames, acquired from 40 to 60 min after injection, and the ^{18}F-FDG image acquisition consisted of four 2-min dynamic frames, acquired from 30 to 38 min after injection. Standard corrections were applied.

PiB and ^{18}F-FDG Production

PiB was synthesized as described elsewhere (*25*). The general ^{11}C-labeling method used was an adaptation of that described by Solbach et al. (*26*). The ^{11}C-PiB product was analyzed by high-performance liquid chromatography to determine radiochemical purity, chemical purity, and specific activity. Endotoxin, pH, and sterility testing were performed. ^{18}F-FDG from ongoing daily production, undergoing the same quality-control testing as was done for PiB, was used for this study.

PiB and ^{18}F-FDG Safety

No adverse events were detected. All subjects or their caregivers were asked in a follow-up phone call about adverse events attributable to the PET scans done as part of this study. Specifically, the following text was used: "Do you have any unexpected pain, tenderness, redness, or swelling in the arm where the injections were performed? Have you had any new fever, rash, breathing difficulties, diarrhea, headache, or muscle pain since your PET scans? If so, how many times, has it interfered with your normal daily activity, and have you needed to see anyone about it or take medications for it?" In all cases, subjects answered no.

Image Analysis

The automated anatomic labeling atlas (*27*) was modified in-house to contain the following labeled regions: right and left parietal, posterior cingulate or precuneus, temporal, prefrontal, orbitofrontal, anterior cingulate, thalamus, striatum, primary sensory–motor, occipital, primary visual, cerebellum, and pons. The high-resolution, T1-weighted, single-subject brain image (*27*) that the atlas was drawn on was normalized to the Montreal Neurologic Institute (MNI) template using the unified segmentation method in SPM5 (*28*), giving a discrete cosine transformation, say F, which normalizes the atlas brain to the MNI template space. The static PiB and ^{18}F-FDG image volumes of each subject were coregistered to the subject's own T1-weighted MRI scan, using a 6 degree-of-freedom affine registration with mutual information cost function. Each MRI scan was then spatially normalized to the MNI template using the unified segmentation model of SPM5 (*28*), giving a discrete cosine transformation, say G_i, which normalizes the MRI of subject i to the MNI template. Then for each subject, the composite transformation $G_i^{-1}(F(.))$ was applied to the atlas to warp the atlas to the subject's anatomic space. Atlas-based parcellation of PiB and ^{18}F-FDG images was, therefore, performed in subject space, to avoid interpolation effects caused by spatial normalization when quantifying PiB and ^{18}F-FDG uptake by region of interest (ROI). For each subject, the sum of the native-space-segmented gray matter (GM) and white matter probability maps generated from the unified segmentation routine was thresholded at a value of 0 to create a binary brain mask. Each subject's brain mask was then multiplied by the subject-specific warped atlas, to generate a custom brain atlas for each subject, parcellated into the aforementioned ROIs. This step was performed to minimize inclusion of cerebrospinal fluid (CSF) in statistics of all ROIs. Statistics on image voxel values were extracted from each labeled cortical ROI in the atlas.

Atrophy Correction

In 1 variation of the automated ROI parcellation algorithm, PVC was performed on the PiB and ^{18}F-FDG images, using a 2-compartment model. Each subject's PiB and ^{18}F-FDG images were coregistered with a 6 degree-of-freedom affine registration to that subject's MRI scan, which was then simultaneously spatially normalized and segmented into GM, WM, and CSF compartments, using the unified segmentation method of SPM5. The GM and WM segmentations were saved in the subject's native space and combined to form a brain tissue probability mask, which was then resampled to the resolution of the PiB image and smoothed with a 6 mm full width at half maximum gaussian filter, to approximate the point spread function of the PET camera. Finally each PiB and ^{18}F-FDG PET voxel was divided by the corresponding value in this smoothed brain mask, in a manner similar to that recommended by Meltzer et al. (*29*) for ^{18}F-FDG PET images.

Cortical ROI Ratios

PiB ROI ratios were calculated by dividing each target region cortical ROI median value by the median value in the cerebellar GM ROI of the atlas. A global cortical PiB uptake summary measure was formed by combining the prefrontal, orbitofrontal, parietal, temporal, anterior cingulate, and posterior cingulate or precuneus ratio values for each subject. This measure was determined by the clinical expectations of abnormal regions and selection of regions with the most prominent PiB groupwise separation, as we have done previously (*6*) (Fig. 2). ^{18}F-FDG ratios were calculated by dividing each target region cortical ROI value by the median value in the pons ROI of the atlas. A global cortical ^{18}F-FDG uptake

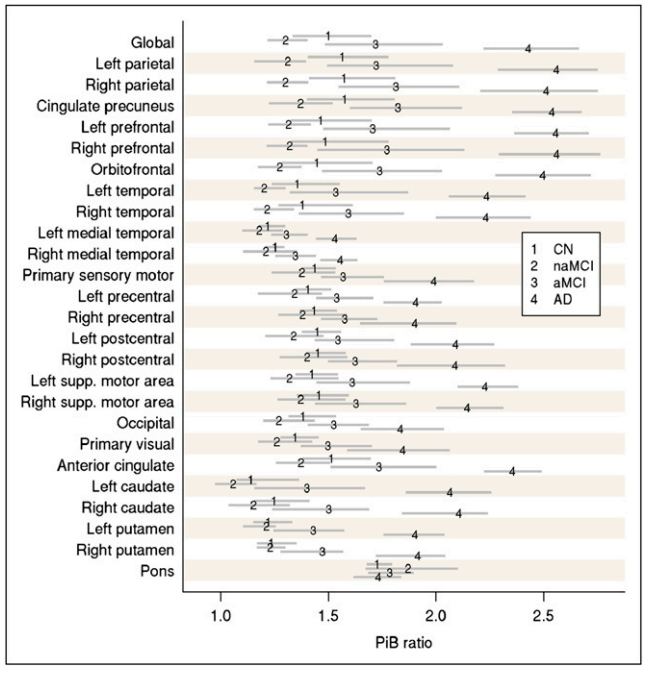

FIGURE 2. Groupwise estimated average ROI-to-cerebellum ratio on PiB PET (numerals 1–4) with 95% nonparametric confidence intervals (gray lines). Average used is pseudo-median, which is defined as median of midpoints of all possible pairs of observations in group. CN = controls; supp. = superior.

summary measure was formed by combining the parietal, temporal, and posterior cingulate or precuneus ratio values for each subject. This measure was determined by selecting regions with the most prominent ^{18}F-FDG groupwise separation (Fig. 3). These regions were similar to those identified by previous authors (*14*) as the most discriminating regions for the 2 PET scans.

SUV Determination

We determined the SUVs normalized for body weight and decay-corrected dose of each target cortical ROI. Cortical ROI median SUVs were recorded and compared with cortical or reference region values described above for both ^{18}F-FDG and PiB. The SUVs were calculated as:

$$\text{SUV} = \frac{\text{median ROI activity (MBq/mL)}}{\text{injected dose (MBq/mL)/body weight (g)}}$$

MRI Methods

All MRI studies were performed with a standardized imaging protocol. All subjects were imaged at 3 T with a 3-dimensional magnetization prepared rapid acquisition gradient-echo imaging sequence as used previously (*6*). Images were interpreted in a setting masked from clinical information to assess for anatomic abnormalities. All subjects' MR images were normalized and segmented using the unified segmentation model in SPM5 with custom elderly tissue probability maps developed in-house (*30*). The normalization parameters obtained were saved for later use in PET data analysis and ROI determinations.

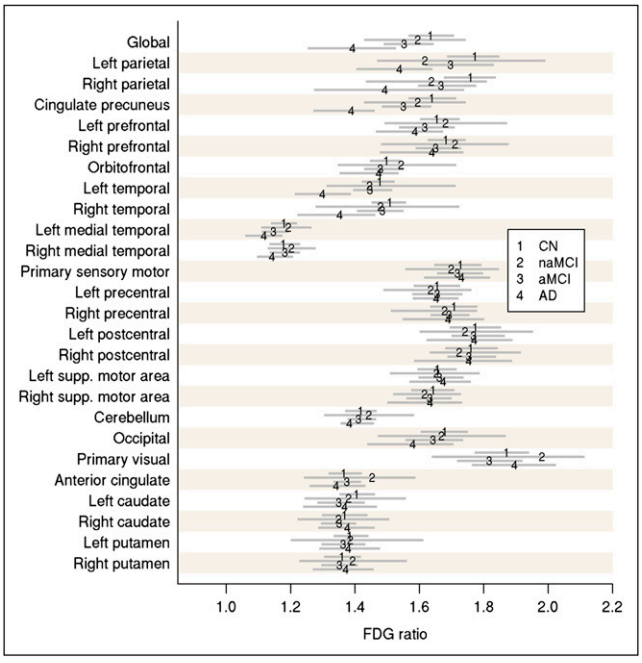

FIGURE 3. Groupwise estimated average ROI-to-pons ratio on ^{18}F-FDG PET (numerals 1–4) with 95% nonparametric confidence intervals (gray lines). Average used is pseudomedian. CN = controls; supp. = superior.

Statistical Methods

We used the Fisher exact test to assess differences in proportions on categoric variables across the 4 subject groups, investigating cortical ratios and SUVs, both with and without PVC, for both PiB and ^{18}F-FDG. We used nonparametric methods to compare groups on imaging and cognitive impairment due to skewness in the distributions. Specifically, the Kruskal–Wallis test was used to evaluate differences across the 4 groups, whereas 2-sample comparisons were performed using Wilcoxon rank sum tests. A 1-sample Wilcoxon signed rank test gives rise to a distribution-free estimate of central tendency and a 95% confidence interval, which we used to compare within-group averages at the ROI level (*31*). The ability of a measure to discriminate between controls and AD was assessed using the area under the ROC curve. *P* values for this 2-sample comparison are reported from the more powerful, but equivalent, 2-sample Wilcoxon rank sum test. We used proportional odds logistic regression to assess the complementary effects of PiB and ^{18}F-FDG on the odds of progressing along the cognitive spectrum represented by the control, aMCI, and AD groups. All tests were performed 2-sided.

RESULTS

PiB

The results suggest significant discrimination ($P < 0.05$) between controls and AD, naMCI and aMCI, naMCI and AD, and aMCI and AD using PiB PET. This discrimination was seen in both partial-volume–corrected and –noncorrected cortical ratio and SUV measurements. PVC led to a small positive bias. The pairwise comparisons of the global PiB cortical ratios and SUVs were not statistically different when evaluated with or without PVC. Notably, similar discriminatory performance was seen between cortical ratio measurements and SUV measurements (Fig. 4). Areas under the ROC curve for controls versus AD subjects (Table 1) reflected the same findings, suggesting a normalization to cerebellum or SUV measurements for PiB could obtain the same diagnostic accuracy.

^{18}F-FDG

The result suggests significant discrimination ($P < 0.05$) between controls and AD, naMCI and AD, and aMCI and AD using ^{18}F-FDG PET. This was seen in both partial-volume–corrected and –noncorrected and cortical ratio measurements. The SUV measurements did not attain statistically significant separation between any of the groups, with or without PVC (Fig. 5). The pairwise comparisons of the global ^{18}F-FDG cortical ratios and SUVs were not statistically different when evaluated with or without PVC. For global ^{18}F-FDG, the ROC areas also showed that pons normalization was superior to SUV measurements in accuracy (Table 1). The ability to discriminate controls from AD was modestly improved for PiB (ROC area, 0.92), as compared with ^{18}F-FDG (ROC area, 0.84), although this was not a statistically significant difference. The improved discrimination between groups by PiB can be seen visually. Figure 6 shows mean images of all subjects in each group for ^{18}F-FDG and PiB scans. The visual separation of the groups is more distinct with PiB.

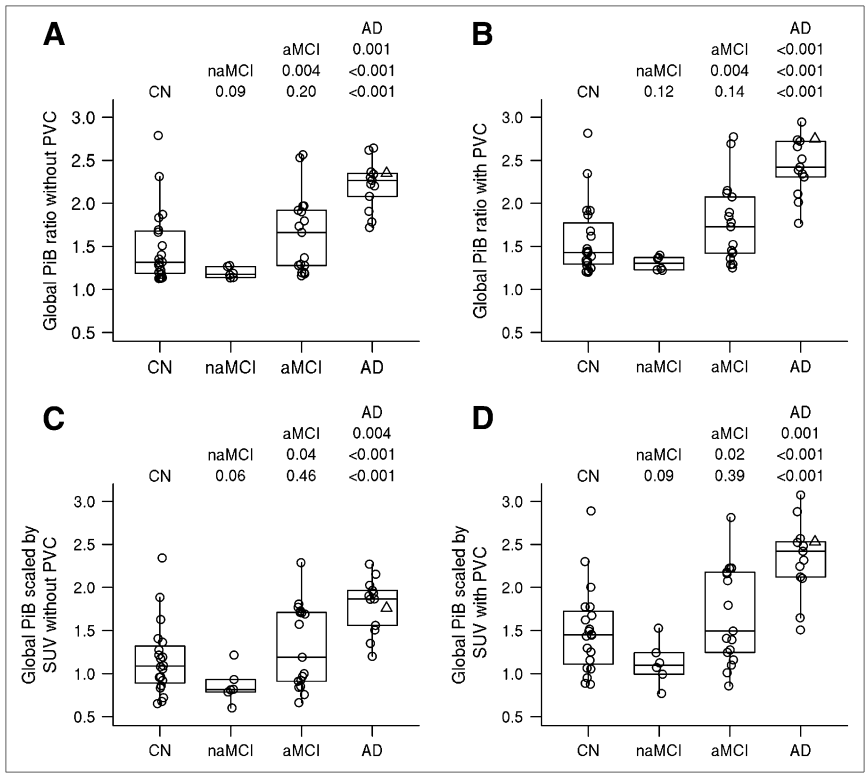

FIGURE 4. Groupwise differences in PiB using 4 approaches. Individual values are superimposed over box plot, indicating median and quartiles. AD subject illustrated in Figure 1 is indicated by a △. At top of each panel are Wilcoxon rank sum test *P* values from all pairwise comparisons. (A) Global cortical PiB-to-cerebellum ratio without PVC. (B) Global cortical PiB-to-cerebellum ratio with PVC. (C) Global cortical PiB scaled by SUV without PVC. (D) Global cortical PiB scaled by SUV with PVC.

The slightly elevated PiB uptake in the control group relative to the naMCI group is likely due to the small contribution from positive PiB cases in the healthy control.

PiB and ^{18}F-FDG Interaction

We used proportional odds logistic regression to determine whether using both tests could improve our groupwise discrimination along the cognitive spectrum represented by the control, aMCI, and AD groups. Global PiB with PVC significantly discriminated among the groups (generalized area under the curve [AUC], 0.79; $P < 0.001$). Likewise, global ^{18}F-FDG with PVC significantly discriminated among the groups (generalized AUC, 0.74; $P < 0.001$). When a model is fit that includes global PiB, global ^{18}F-FDG, and the interaction, the interaction is significant ($P < 0.03$) and generalized AUC increases to 0.84. At a higher level of ^{18}F-FDG (i.e., the 75th percentile), moving from the 25th percentile to the 75th percentile on PiB can be expected to quadruple a subject's odds of progression to a more impaired diagnosis. However, with ^{18}F-FDG at the 25th percentile, the effect of this increase in PiB is more than 5 times greater. In other words, high ^{18}F-FDG may mitigate the negative effect of higher PiB. High PiB, given low ^{18}F-FDG, is quite disadvantageous. The ^{18}F-FDG effect similarly depends on the subject's PiB level. At good PiB levels equivalent to the 25th percentile, there is no significant increase in odds of a more impaired diagnosis as ^{18}F-FDG drops from the 75th to the 25th percentile. However, at high PiB levels equivalent to the 75th percentile, the odds of a more impaired diagnosis increased over 6-fold when ^{18}F-FDG drops from the 75th to the 25th percentile.

MCI Subjects

Subjects with aMCI ($n = 17$) had significant amyloid uptake as compared with naMCI subjects ($n = 6$), and the groups showed significant pairwise separation (Fig. 4). This was seen for PiB, whereas the ^{18}F-FDG measures were indistinguishable (Fig. 5). The naMCI subjects did not show PiB accumulation and were not statistically different from the control group with either PiB or ^{18}F-FDG by any of the methods used (Fig. 6). Table 2 shows the subject

TABLE 1. Area under the ROC Curve for Controls Versus AD Subjects

Method	AUC	95% confidence interval	*P**
Global PiB			
Cerebellum-scaled with no PVC	0.90	0.79, 1.00	<0.001
Cerebellum-scaled with PVC	0.92	0.82, 1.00	<0.001
SUV-scaled with no PVC	0.88	0.76, 1.00	<0.001
SUV-scaled with PVC	0.90	0.78, 1.00	<0.001
Global ^{18}F-FDG			
Pons-scaled with no PVC	0.89	0.78, 1.00	<0.001
Pons-scaled with PVC	0.83	0.68, 0.98	<0.001
SUV-scaled no PVC	0.71	0.52, 0.89	0.05
SUV-scaled with PVC	0.68	0.49, 0.88	0.08

*Based on 2-sided Wilcoxon rank sum test.

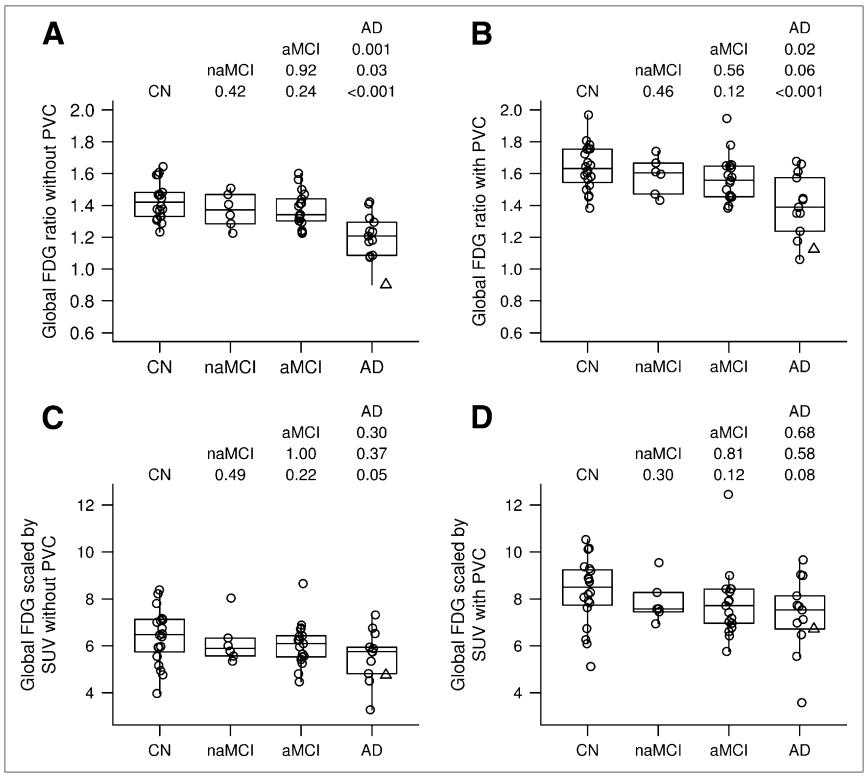

FIGURE 5. Groupwise differences in ^{18}F-FDG using 4 approaches. Individual values are superimposed over box plot, indicating median and quartiles. AD subject illustrated in Figure 1 is indicated by a △. At top of each panel are Wilcoxon rank sum test *P* values from all pairwise comparisons. (A) Global cortical ^{18}F-FDG-to-pons ratio without PVC. (B) Global cortical ^{18}F-FDG-to-pons ratio with PVC. (C) Global cortical ^{18}F-FDG SUV without PVC. (D) Global cortical ^{18}F-FDG SUV with PVC.

demographics, with subjects subcategorized into those who were PiB-positive and those who were PiB-negative. A ratio greater than 1.5 was used to indicate PiB positivity and was defined using the methods we have reported previously (*6*). Interestingly, there is significant attention or executive and visuospatial scoring differences (abnormalities) in the naMCI group (who were all PiB-negative) versus the aMCI PiB-positive group. Although the memory scores for the naMCI group were lower than those of the controls, the consensus diagnosis that assigns the final diagnostic category listed all of these subjects as not showing memory impairment, and hence they were classified as naMCI subjects. The aMCI PiB-negative and aMCI PiB-positive subjects did not score significantly differently, as one might expect, although the attention or executive score differences approach significance.

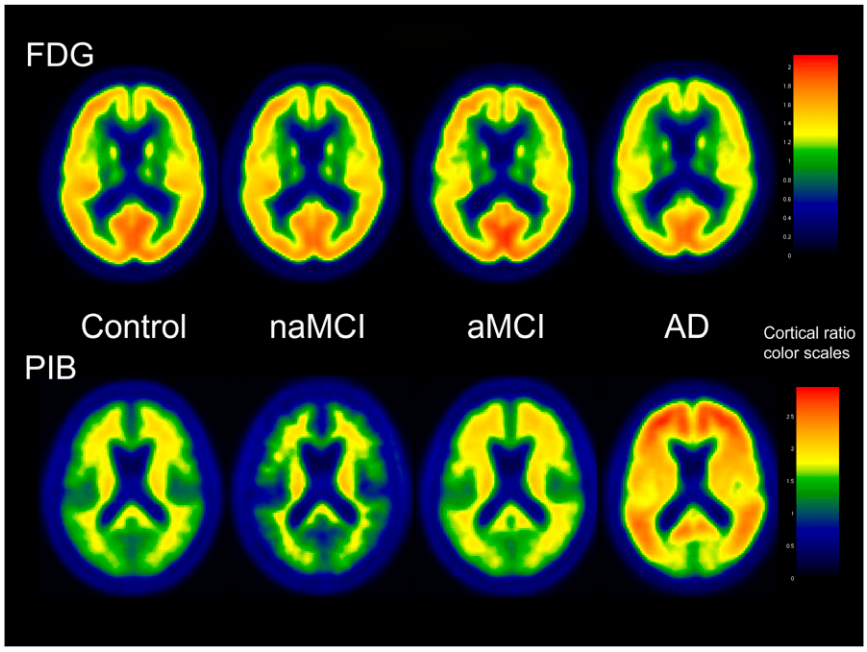

FIGURE 6. ^{18}F-FDG and PiB group mean images for control, naMCI, aMCI, and AD subjects showing better visual separation of groups using PiB. Scaling shown to right using pons and cerebellar normalization, respectively. Regions with activity similar to these regions of normalization color in 1.0 color ranges (green), whereas regions with greater uptake show up in yellow and red. Color scaling is slightly different for ^{18}F-FDG and PiB groups given different range of cortical ratios.

DISCUSSION

We found that although PiB and ^{18}F-FDG showed similar accuracy in separating cognitively impaired subjects into the defined clinical categories, there was a trend for improved accuracy with PiB. This improved accuracy was most significantly demonstrated by a pairwise separation of naMCI and aMCI subjects. There was also a slight improvement in ROC curve data from PiB, compared with ^{18}F-FDG, in characterizing control and probable-AD groups. The improved pairwise separation with PiB can be seen graphically in Figures 4 and 5 and is also demonstrated by a greater difference in multiple cortical regions in which such separation would be expected in the subject groups (Figs. 2 and 3, respectively). The percentage of change between the control and AD groups is much greater for PiB than for ^{18}F-FDG in different brain ROIs in which the separation is expected. For example, the change from control to AD is a 70% increase generally for PiB, whereas it is in the range of a 20% decrease for ^{18}F-FDG. These factors likely contribute to the improved pairwise separation for PiB. These findings translate into better visual separation of the groups by PiB (Fig. 6).

Our study is supportive of previously published work by Ng et al. (*14*); in this paper, healthy (n = 15) and probable-AD subjects (n = 15) were included. Although the AD subjects had mild-to-moderate dementia, no early cognitively impaired subjects, such as the MCI subjects, were included. In addition, in the study by Ng et al. (*14*), visual interpretation was compared with cortical ratios, and they were found to be equivalent in accuracy. Cerebellar regions were used for both PiB and ^{18}F-FDG normalization. There was no mention of using atrophy correction, nor did the analysis use any additional normalization strategy such as dose or weight normalization. Similar to our findings, PiB was found to be superior to ^{18}F-FDG in accurately characterizing healthy and AD subjects.

Given these findings, the question could be posed about the role of ^{18}F-FDG and PiB in dementia imaging. Are they complementary? Recently we showed that PiB and MRI hippocampal W scores were complementary in discriminating among subjects along the cognitive spectrum ranging from control to aMCI to AD (*6*). Using the same ordinal logistic regression approach but with this slightly larger group, we found that ^{18}F-FDG and PiB are in fact complementary and that we significantly improve our group-wise discrimination when we account for a subject's PiB and ^{18}F-FDG values. As was found to be the case with PiB and MRI hippocampal W score, the significant interaction between PiB and ^{18}F-FDG means that the effect of 1 PET measure on the odds of a more cognitively impaired diagnosis depends on the level of the other measure.

Image Analysis Methods

We evaluated various methods of analysis of PiB and ^{18}F-FDG PET data in this project to assess and optimize the performance of each test. The performance impact of using PVC in evaluating PiB and ^{18}F-FDG images in character-

TABLE 2. Subject Summary Statistics Subcategorized by Global PiB: Positive and Negative

Statistic	CN− (n = 14)	CN+ (n = 6)	aMCI− (n = 8)	aMCI+ (n = 9)	naMCI− (n = 6)	AD+ (n = 13)	Two-sided rank sum P: aMCI+ vs. aMCI−	aMCI+ vs. naMCI	aMCI− vs. naMCI
Age									
Median	75.0	78.0	82.0	73.0	75.5	79.0	0.09	0.41	0.33
Range	72.0–88.0	73.0–90.0	76.0–87.0	56.0–87.0	70.0–90.0	54.0–91.0			
Education									
Median	13.5	16.0	12.0	16.0	12.0	16.0	0.083	0.12	0.55
Range	12.0–20.0	12.0–20.0	11.0–19.0	12.0–20.0	8.0–19.0	8.0–20.0			
Memory									
Median	10.3	10.5	7.4	6.0	7.9	4.1	0.34	0.098	0.65
Range	8.2–12.8	6.6–12.6	4.7–10.3	3.9–9.1	6.4–8.9	2.4–5.9			
Language									
Median	10.8	13.3	9.3	9.5	9.3	5.4	0.77	0.55	0.79
Range	8.5–15.0	10.5–14.0	7.0–12.5	7.5–12.0	6.3–12.5	2.0–12.3			
Attention									
Median	10.3	11.2	8.3	11.0	6.4	5.6	0.067	0.005	0.045
Range	7.7–14.7	7.3–15.3	5.7–12.0	6.7–11.8	2.7–8.3	2.7–11.3			
Visuospatial									
Median	10.5	12.8	10.8	13.0	6.3	8.0	0.17	0.004	0.002
Range	6.5–14.5	7.5–15.0	9.0–15.0	6.5–15.5	5.0–8.5	2.0–14.0			
Short test score									
Median	35.0	35.0	32.0	32.0	30.5	20.0	0.52	0.048	0.48
Range	28.0–38.0	30.0–38.0	22.0–35.0	30.0–35.0	23.0–33.0	7.0–34.0			
CDR sum of boxes									
Median	0.0	0.0	1.0	1.5	0.8	5.5	0.17	0.31	0.90
Range	0.0–0.5	0.0–0.5	0.0–2.5	0.5–4.5	0.0–4.5	1.5–13.0			

izing subjects with memory impairment was evaluated. We did not find any significant difference between the 2 methods. Small positive biases were seen with PVC, as could be expected. If any conclusion could be made it would be based on subtle trends and would favor using PVC in the data analysis of PiB and ^{18}F-FDG PET. Other methods of PVC could be entertained. These data were based on mildly impaired subjects, and subjects with more severe atrophy could differ more significantly.

We found that PiB PET data analyzed using cortical ratios or SUVs were indistinguishable statistically in terms of pairwise group separation or controls versus AD characterization accuracy. This was not the case for ^{18}F-FDG. This finding may provide data to support SUV image analysis as an alternative evaluation for subjects who have noticeable PiB accumulation in regions such as the cerebellum that are used for cortical region ratio calculation. Also, in respect to future clinical use of the test, as most PET systems can now provide such SUV data in regions selected on the view screens of interpretation workstations, quick regional quantification could be considered during clinical reading as an aid in interpretation.

MCI Subjects

MCI subjects are of great interest in the context of studying imaging biomarkers of early AD. However, data regarding the performance of PiB PET are limited in MCI subjects. The ability of ^{18}F-FDG PET to accurately characterize MCI subjects is also of some debate. Some reports have shown that only 50% of MCI cases have reduced ^{18}F-FDG uptake (*1,32–34*), whereas others have found more consistent abnormalities when particular at-risk areas, such as the mesial temporal lobes, are specifically evaluated (*1,32–37*). Forsberg et al. recently reported a high likelihood of conversion to probable AD in those MCI subjects with positive PiB scans (7 of 20) (*38*). It appears likely, nonetheless, that MCI subjects with elevated cortical PiB uptake or reduced ^{18}F-FDG uptake are more likely to convert to AD.

A recent publication presented results on PiB and ^{18}F-FDG imaging. In this report ^{18}F-FDG was superior in the classification of controls versus MCI subjects, and PiB and ^{18}F-FDG were similar in their ability to classify AD (*39*). Various differences between that study and ours may explain the seemingly differing results, including the use by that study of a fully quantitative ^{18}F-FDG metabolic glucose rate calculation and a relatively small group of 7 healthy subjects.

In considering the evaluation of MCI subjects, probable AD may not develop clinically in a significant number of subjects who carry an MCI diagnosis, and only longitudinal study can accurately assess the diagnostic performance or pathophysiologic importance of either ^{18}F-FDG or PiB PET in this cohort. Subcategorizing the MCI cohort as we have done may, therefore, be a better way in the short term for characterizing the risk of AD developing in this cohort and be of more help in understanding the imaging findings in the MCI group.

MCI subjects can be characterized as amnestic or nonamnestic, as described above, with each subtype likely having different risks of conversion to AD. No reports to date have evaluated PiB and ^{18}F-FDG in naMCI and aMCI subjects. In this report, we evaluated MCI subjects with presumed higher risk of converting to probable AD (aMCI) relative to lower-risk naMCI subjects (*40*). We saw a clear separation of the groups using PiB imaging only with the naMCI subjects having no amyloid accumulation. Granted, the number of subjects was small, but this may suggest that the aMCI subjects exhibiting amyloid deposition, in whom the risk of converting to AD is highest, have early physiologic preservation of glucose metabolism. Therefore, hypometabolism may occur after the amyloid insult. If this is true, the combination of the 2 PET tests may provide a way to study such theories as brain reserve in the presence of amyloid in the pathogenesis of AD (*41*). Clearly, larger correlative studies would be needed to evaluate this possibility.

In addition, significant attention or executive and visuospatial scoring differences (abnormalities) in the naMCI group (who were all PiB-negative) versus the aMCI PiB-positive group were seen. This could suggest that the naMCI group seen here reflected subjects with evolving Lewy body disease because impairment in the domains of attention or executive and visuospatial functioning are characteristic of dementia with Lewy bodies (*42*). These data highlight the difficulty in clinical decision making and hence the importance of new accurate imaging methods such as PiB PET. These naMCI subjects had low memory scores, and the consensus diagnosis favored less emphasis on the memory score and more emphasis on attention or visuospatial compromise or other clinical findings and listed them as not being memory-impaired. This is likewise a confirmatory finding on the heterogeneous nature of the MCI group, as has been noted on imaging reports previously, and provides a better understanding of the variable PET results that have been seen (*9*) in MCI subjects when they have been studied as a homogeneous group.

CONCLUSION

In classifying subjects with memory impairment, PiB showed slightly better separation of subjects, compared with ^{18}F-FDG PET. Significantly better group discrimination in naMCI and aMCI subjects by PiB over ^{18}F-FDG may suggest early amyloid deposition before cerebral metabolic perturbation. The use of PVC for evaluating PiB and ^{18}F-FDG PET data in subjects with memory impairment is not necessary to provide equivalent group separation. The use of cortical-to-reference ratios (SUVR) provides equivalent accuracy to normalization to dose and body weight SUV calculation for PiB. Cortical-to-reference ratios are superior for ^{18}F-FDG data analysis.

REFERENCES

1. Chetelat G, Desgranges B, de la Sayette V, Viader F, Eustache F, Baron JC. Mild cognitive impairment: can FDG-PET predict who is to rapidly convert to Alzheimer's disease? *Neurology.* 2003;60:1374–1377.
2. Drzezga A, Grimmer T, Henriksen G, et al. Imaging of amyloid plaques and cerebral glucose metabolism in semantic dementia and Alzheimer's disease. *Neuroimage.* 2008;39:619–633.
3. Engler H, Forsberg A, Almkvist O, et al. Two-year follow-up of amyloid deposition in patients with Alzheimer's disease. *Brain.* 2006;129:2856–2866.
4. Tuszynski MH, Thal L, Pay M, et al. A phase 1 clinical trial of nerve growth factor gene therapy for Alzheimer disease. *Nat Med.* 2005;11:551–555.
5. Klunk WE, Engler H, Nordberg A, et al. Imaging brain amyloid in Alzheimer's disease with Pittsburgh Compound-B. *Ann Neurol.* 2004;55:306–319.
6. Jack CR Jr, Lowe VJ, Senjem ML, et al. ^{11}C PiB and structural MRI provide complementary information in imaging of Alzheimer's disease and amnestic mild cognitive impairment. *Brain.* 2008;131:665–680.
7. Kemppainen NM, Aalto S, Wilson IA, et al. Voxel-based analysis of PET amyloid ligand [^{11}C]PIB uptake in Alzheimer disease. *Neurology.* 2006;67:1575–1580.
8. Price JC, Klunk WE, Lopresti BJ, et al. Kinetic modeling of amyloid binding in humans using PET imaging and Pittsburgh Compound-B. *J Cereb Blood Flow Metab.* 2005;25:1528–1547.
9. Rowe CC, Ng S, Ackermann U, et al. Imaging beta-amyloid burden in aging and dementia. *Neurology.* 2007;68:1718–1725.
10. Mintun MA, Larossa GN, Sheline YI, et al. [^{11}C]PIB in a nondemented population: potential antecedent marker of Alzheimer disease. *Neurology.* 2006;67:446–452.
11. Forsberg A, Engler H, Almkvist O, et al. PET imaging of amyloid deposition in patients with mild cognitive impairment. *Neurobiol Aging.* 2008;29:1456–1465.
12. Petersen RC, Parisi JE, Dickson DW, et al. Neuropathologic features of amnestic mild cognitive impairment. *Arch Neurol.* 2006;63:665–672.
13. Petersen RC, O'Brien J. Mild cognitive impairment should be considered for DSM-V. *J Geriatr Psychiatry Neurol.* 2006;19:147–154.
14. Ng S, Villemagne VL, Berlangieri S, et al. Visual assessment versus quantitative assessment of ^{11}C-PIB PET and ^{18}F-FDG PET for detection of Alzheimer's disease. *J Nucl Med.* 2007;48:547–552.
15. Lopresti BJ, Klunk WE, Mathis CA, et al. Simplified quantification of Pittsburgh Compound B amyloid imaging PET studies: a comparative analysis. *J Nucl Med.* 2005;46:1959–1972.
16. Verkkoniemi A, Kalimo H, Paetau A, et al. Variant Alzheimer disease with spastic paraparesis: neuropathological phenotype. *J Neuropathol Exp Neurol.* 2001;60:483–492.
17. Singleton AB, Hall R, Ballard CG, et al. Pathology of early-onset Alzheimer's disease cases bearing the Thr113-114ins presenilin-1 mutation. *Brain.* 2000;123:2467–2474.
18. Bird TD, Lampe TH, Nemens EJ, et al. Characteristics of familial Alzheimer's disease in nine kindreds of Volga German ancestry. *Prog Clin Biol Res.* 1989;317:229–234.
19. Mann DM, Jones D, Prinja D, Purkiss MS. The prevalence of amyloid (A4) protein deposits within the cerebral and cerebellar cortex in Down's syndrome and Alzheimer's disease. *Acta Neuropathol.* 1990;80:318–327.
20. American Psychiatric Association. *Diagnostic and Statistical Manual of Mental Disorders: DSM-III.* 3rd ed., rev. Washington, DC: American Psychiatric Association; 1987.
21. McKhann G, Drachman D, Folstein M, Katzman R, Price D, Stadlan EM. Clinical diagnosis of Alzheimer's disease: report of the NINCDS-ADRDA work group under the auspices of Department of Health and Human Services Task Force on Alzheimer's Disease. *Neurology.* 1984;34:939–944.
22. Winblad B, Palmer K, Kivipelto M, et al. Mild cognitive impairment: beyond controversies, towards a consensus: report of the International Working Group on Mild Cognitive Impairment. *J Intern Med.* 2004;256:240–246.
23. Morris JC. The Clinical Dementia Rating (CDR): current version and scoring rules. *Neurology.* 1993;43:2412–2414.
24. Lucas JA, Ivnik RJ, Smith GE, et al. Mayo's older Americans normative studies: category fluency norms. *J Clin Exp Neuropsychol.* 1998;20:194–200.
25. Mathis CA, Wang Y, Holt DP, Huang GF, Debnath ML, Klunk WE. Synthesis and evaluation of ^{11}C-labeled 6-substituted 2-arylbenzothiazoles as amyloid imaging agents. *J Med Chem.* 2003;46:2740–2754.
26. Solbach C, Uebele M, Reischl G, Machulla HJ. Efficient radiosynthesis of carbon-11 labelled uncharged thioflavin T derivatives using [^{11}C]methyl triflate for beta-amyloid imaging in Alzheimer's disease with PET. *Appl Radiat Isot.* 2005;62:591–595.
27. Tzourio-Mazoyer N, Landeau B, Papathanassiou D, et al. Automated anatomical labeling of activations in SPM using a macroscopic anatomical parcellation of the MNI MRI single-subject brain. *Neuroimage.* 2002;15:273–289.
28. Ashburner J, Friston KJ. Voxel-based morphometry: the methods. *Neuroimage.* 2000;11:805–821.
29. Meltzer CC, Cantwell MN, Greer PJ, et al. Does cerebral blood flow decline in healthy aging? A PET study with partial-volume correction. *J Nucl Med.* 2000;41:1842–1848.
30. Vemuri P, Gunter JL, Senjem ML, et al. Alzheimer's disease diagnosis in individual subjects using structural MR images: validation studies. *Neuroimage.* 2008;39:1186–1197.
31. Hollander M, Wolfe DA. *Nonparametric Statistical Methods.* New York, NY: Wiley; 1999.
32. Mosconi L, Tsui WH, De Santi S, et al. Reduced hippocampal metabolism in MCI and AD: automated FDG-PET image analysis. *Neurology.* 2005;64:1860–1867.
33. Drzezga A, Grimmer T, Riemenschneider M, et al. Prediction of individual clinical outcome in MCI by means of genetic assessment and ^{18}F-FDG PET. *J Nucl Med.* 2005;46:1625–1632.
34. Anchisi D, Borroni B, Franceschi M, et al. Heterogeneity of brain glucose metabolism in mild cognitive impairment and clinical progression to Alzheimer disease. *Arch Neurol.* 2005;62:1728–1733.
35. Mosconi L, Perani D, Sorbi S, et al. MCI conversion to dementia and the APOE genotype: a prediction study with FDG-PET. *Neurology.* 2004;63:2332–2340.
36. de Leon MJ, Convit A, Wolf OT, et al. Prediction of cognitive decline in normal elderly subjects with 2-[^{18}F]fluoro-2-deoxy-D-glucose/poitron-emission tomography (FDG/PET). *Proc Natl Acad Sci USA.* 2001;98:10966–10971.
37. Mosconi L. Brain glucose metabolism in the early and specific diagnosis of Alzheimer's disease: FDG-PET studies in MCI and AD. *Eur J Nucl Med Mol Imaging.* 2005;32:486–510.
38. Forsberg A, Engler H, Almkvist O, et al. PET imaging of amyloid deposition in patients with mild cognitive impairment. *Neurobiol Aging.* 2008;29:1456–1465.
39. Li Y, Rinne JO, Mosconi L, et al. Regional analysis of FDG and PIB-PET images in normal aging, mild cognitive impairment, and Alzheimer's disease. *Eur J Nucl Med Mol Imaging.* 2008;35:2169–2181.
40. Aggarwal NT, Wilson RS, Beck TL, Bienias JL, Bennett DA. Mild cognitive impairment in different functional domains and incident Alzheimer's disease. *J Neurol Neurosurg Psychiatry.* 2005;76:1479–1484.
41. Roe CM, Mintun MA, D'Angelo G, Xiong C, Grant EA, Morris JC. Alzheimer disease and cognitive reserve: variation of education effect with carbon 11-labeled Pittsburgh Compound B uptake. *Arch Neurol.* 2008;65:1467–1471.
42. McKeith IG, Dickson DW, Lowe J, et al. Diagnosis and management of dementia with Lewy bodies: third report of the DLB Consortium. *Neurology.* 2005;65:1863–1872.

JNM The Journal of NUCLEAR MEDICINE

Comparison of ^{18}F-FDG and PiB PET in Cognitive Impairment

Val J. Lowe, Bradley J. Kemp, Clifford R. Jack, Jr., Matthew Senjem, Stephen Weigand, Maria Shiung, Glenn Smith, David Knopman, Bradley Boeve, Brian Mullan and Ronald C. Petersen

J Nucl Med. 2009;50:878-886.
Published online: May 14, 2009.
Doi: 10.2967/jnumed.108.058529

The Journal of Nuclear Medicine is published monthly.
SNMMI | Society of Nuclear Medicine and Molecular Imaging
1850 Samuel Morse Drive, Reston, VA 20190.
(Print ISSN: 0161-5505, Online ISSN: 2159-662X)

SNMMI SOCIETY OF NUCLEAR MEDICINE AND MOLECULAR IMAGING